Stem Cell Research (2014) 12, 646–658

Available online at www.sciencedirect.com

ScienceDirect

www.elsevier.com/locate/scr

Basic fibroblast growth factor modifies the hypoxic response of human bone marrow stromal cells by ERK-mediated enhancement of HIF-1α activity

Zsolt Fábián[a,b], Sivaramakrishnan Ramadurai[a,c], Georgina Shaw[b], Heinz-Peter Nasheuer[a,c], Walter Kolch[d,e], Cormac Taylor[d,e], Frank Barry[a,b,*]

[a] Systems Biology Ireland, National University of Ireland Galway, Galway, Ireland
[b] Regenerative Medicine Institute, National University of Ireland Galway, Galway, Ireland
[c] School of Natural Sciences, National University of Ireland Galway, Galway, Ireland
[d] Systems Biology Ireland, University College Dublin, Belfield, Dublin 4, Ireland
[e] Conway Institute, University College Dublin, Dublin, Ireland

Received 9 November 2013; received in revised form 24 February 2014; accepted 26 February 2014
Available online 6 March 2014

Abstract Human bone marrow stromal cells (hBMSCs, also known as bone marrow-derived mesenchymal stem cells) are promising tools for the cellular therapy of human pathologies related to various forms of hypoxia. Although the current concepts of their clinical use include the expansion of hBMSC in standard cell culture conditions, the effect of the mitogen-driven *ex vivo* expansion on the adaptation to the hypoxic environment is unknown. Here, we provide data that the basic fibroblast growth factor (FGF2) enhances the induction of a wide range of hypoxia-related adaptive genes in hypoxic hBMSCs. We identified that the FGF2 signal is transmitted by the ERK pathway similar to that of hypoxia that also utilises the distal elements of the same signalling machinery including the extracellular signal-regulated kinase 1/2 (ERK1/2) and mitogen-activated protein kinase kinases (MEK1/2) in hBMSCs. We found that the simultaneous activation of ERK1/2 by FGF2 and hypoxia transforms the activation dynamics from oscillatory into sustained one. Activated ERKs co-localise with stabilised hypoxia inducible factor-1α (HIF-1α) followed by the reduction of its nuclear mobility as well as increased DNA binding capacity leading to the up-regulation of hypoxia-adaptive genes. Our findings indicate that the status of the ERK pathway has significant impacts on the molecular adaptation of hBMSCs to the hypoxic milieu.

Introduction

Cultures of human bone marrow stromal cells (hBMSCs, also known as human bone marrow-derived mesenchymal stem

* Corresponding author at: Regenerative Medicine Institute, National University of Ireland Galway, Galway, Republic of Ireland. Fax: +353 91 494 596.
E-mail address: frank.barry@nuigalway.ie (F. Barry).

http://dx.doi.org/10.1016/j.scr.2014.02.007
1873-5061/

cells) contain multipotent cells (bone marrow mesenchymal stem cells) with the capacity to differentiate into a variety of cell types including chondrocytes, osteoblasts or adipocytes (Dominici et al., 2006; Pittenger et al., 1999). They are believed to have a great medical potential in a range of human pathologies especially those that require the regeneration of the bone and cartilage (Robey and Bianco, 2006). Despite the different pathogenesis, local hypoxia is considered to be a critical factor in a number of medical conditions affecting these tissues. In experimental conditions, hBMSCs efficiently adapt to low oxygen environments by adjusting their gene expression and metabolism to the hypoxic conditions that results in enhanced proliferation and differentiation (Grayson et al., 2007; Kanichai et al., 2008). These observations further fuelled the idea that hBMSC cultures are particularly useful for cellular therapy of oxygen-depleted tissues.

The current concepts of the hBMSCs-based cellular therapies include the *in vitro* expansion of the cells for, at least, two reasons. On the one hand, one of the minimal criteria for defining hBMSCs is their adherence to plastic in standard cell culture conditions (Dominici et al., 2006). On the other, *in vivo* studies suggest that a minimum of 10^7–10^{11} transplanted hBMSCs are required for clinically evaluable efficacy (Chen et al., 2004; Macmillan et al., 2009; Mazzini et al., 2010; Perez-Simon et al., 2011). Thus, due to their limited *ex vivo* proliferation capacity, the hBMSC culture media are commonly supplemented with mitogenic factors including the basic fibroblast growth factor (FGF2) (Martin et al., 1997).

The ubiquitously expressed FGF2 is the prototypic member of the paracrine group of human FGFs (Beenken and Mohammadi, 2009). Its endogenous expression is regulated at multiple levels including the alternative translation of polypeptides that eventually differ in size (18–34 kDa), domain structure and intracellular localization (Yu et al., 2007). Although experimental results suggest the function of FGF2 in angiogenesis and the regulation of the vascular tone, its physiological roles remain unclear as $FGF1^{-/-}$ and $FGF2^{-/-}$ double knock-out mice are completely viable and fertile showing only minor defects in brain development, haematopoiesis and wound healing (Cuevas et al., 1991; Fulgham et al., 1999; Miller et al., 2000; Zhou et al., 1998). FGFs signal *via* structurally related cell surface receptors (FGFR1-5) that, apart from FGFR5, function as receptor tyrosine kinases (Mohammadi et al., 2005; Sleeman et al., 2001). The multiple isoforms of FGFR1-3 generated by exon skipping and alternative splicing have different ligand specificity and tissue-specific expression (Eisemann et al., 1991; Johnson et al., 1991). The signalling machinery of FGFs is similarly complex and, based on literature data, linked to the PLCγ1, the PKB/Akt and the ERK pathways alike (Chen et al., 2000; Chikazu et al., 2000; Park et al., 1999). The effects of the 18 kDa species of FGF2 used on hBMSC include the preservation of their fibroblast morphology as well as proliferation and differentiation capacity (Martin et al., 1997). Interestingly, these effects are similar to those of hypoxia on FGF-naïve hBMSCs including the enhanced proliferation, prevented senescence, up-regulated metabolism and, apart from the osteogenic lineages, increased differentiation efficiency (Grayson et al., 2007; Kanichai et al., 2008; Tsai et al., 2011; Volkmer et al., 2010).

The primary intracellular sensors of hypoxia are the prolyl hydroxylase enzymes (PHDs) that, utilising oxygen as co-factor, hydroxylate critical proline residues of their substrates (Willam et al., 2004). PHDs target the basic helix-loop-helix transcription factor hypoxia inducible factor-1 (HIF-1) (Wang et al., 1995). Active HIF-1 consists of one alpha and one beta subunits that are constitutively translated in most cells types (Wang and Semenza, 1995). PHD-mediated prolyl hydroxylation of the alpha subunit, however, induces its ubiquitination and proteasomal degradation preventing the formation of the active HIF-1α/β heterodimers (Chan et al., 2002; Ivan et al., 2002; Masson et al., 2001). In contrast, under hypoxic conditions, PHDs become inactive leading to the accumulation of the functional HIF-1 heterodimers. Once stabilised, active HIF-1 alters the transcriptional pattern to facilitate cellular adaptation to the hypoxic milieu (Majmundar et al., 2010).

Although the molecular machinery orchestrating the biological responses to hypoxia at the transcriptional level is well detailed, the relationship between the FGF2 and hypoxia signalling in hBMSCs has remained unexplored. The similar effects of FGF2 and hypoxia on hBMSC cultures, however, suggest that the two stimuli utilise, at least in part, the same molecular machinery. This raises the question if the use of FGF2 upon the *in vitro* expansion of hBMSCs has an impact on the hypoxic adaptation of the same. We investigated this question by combining methodologies of molecular biology and biophysics. Here, we provide data that FGF2 enhances the expression of genes critical in the metabolic adaptation to hypoxia. We found that both FGF2 and hypoxia signal through the ERK pathway and the two signals are merged upstream of the mitogen activated protein kinase kinase (MEK). The simultaneous activation of the ERK pathway in FGF2-cultured hypoxic hBMSCs leads to altered signalling dynamics and enhanced HIF-1α DNA binding activity. We found that the latter effect is mediated post-translationally by direct interaction of the activated ERK and stabilised HIF-1α proteins. We also provide data that FGF2 not only facilitates the reduction of the nuclear mobility of HIF-1α but also results in modified complex formation in hypoxic cells.

Materials and methods

Cell cultures and chemicals

Plastic adherent human bone marrow stromal cells were obtained from bone marrow aspirates taken from the iliac crest of healthy donors. All procedures were performed with informed consent and approved by the Clinical Research Ethical Committee at University College Hospital, Galway. Bone marrow aspirates were diluted in 1× Dulbecco's Phosphate-Buffered Saline (DPBS; Life Technologies) in 1:1 ratio and centrifuged at 800 *g* for 10 min. Supernatant was removed and cells were re-suspended in 1 × DPBS. Test sample was taken from the suspension, diluted in 1:10 ratio in 1 × DPBS and mononuclear cells were counted using 4% acetic acid (1:1). For FGF2-treated cultures, 8.75×10^6 mononuclear cells per T-175 flask were plated in alpha-Minimum Essential Medium (α-MEM; Life Technologies) containing 10% pre-screened foetal bovine serum (FBS; Hyclone, South Logan, UT, USA), mixture of penicillin/streptomycin (1%) and supplemented with 1 ng/mL recombinant 18 kDa human basic fibroblast growth factor (FGF2; PeproTech, UK). For FGF2-naïve cultures, approximately 4.0×10^7 mononuclear cells per T-175 flask were plated in α-MEM containing 10% pre-screened foetal bovine serum (FBS;

Hyclone, South Logan, UT, USA) and a mixture of penicillin/streptomycin (1%). Cultures were maintained at 37 °C with 95% humidity and 5% CO_2 in the same medium for 5 days. Following incubation, non-adherent cells were washed off with 1× DPBS and fresh medium was added. Colonies of adherent cells usually formed within 9 days were detached using 0.25% trypsin/0.53 mM ethylenediaminete-tetraacetic acid (EDTA) solution. U-2 OS human osteosarcoma cells were maintained in Dulbecco's Modified Eagle Medium (DMEM) with 4500 mg/L glucose and 4 mM L-Glutamine supplemented with 10% heat-inactivated FBS and 1% penicillin/streptomycin. Phenol-red containing culture media was replaced with phenol-red free DMEM supplemented as detailed above 24 h before fluorescent correlation spectroscopy. U-2 OS cells stably expressing the eGFP-tagged HIF-1α were established using the Gateway cloning system (Invitrogen) with HIF-1α cDNA (Genepodia) carrying entry and pIC113-based eGFP vectors (pIC113gw from Prof. K. Sullivan). All chemicals were purchased from Sigma-Aldrich unless otherwise stated. U0126 was purchased from Calbiochem.

Flow cytometry

Isolated hBMSCs (10^5/antibody) were blocked on ice in PBS with 2% FBS for 30 min. After centrifugation the cells were resuspended in 50 μL of phycoerithrin-conjugated antibody (Table S2) and incubated on ice for 30 min. Cells were then washed twice in 1 × DPBS with 2% FBS prior to analysis on a BD FACS Canto II. Data were analysed using FloJo software (Fig. S1A).

Functional characterization of hBMSCs

Functional characterization of hBMSCs was carried out by testing the adipo-, osteo- and chondrogenic capacity of the cells (Figs. S1B–D). Adipogenesis was induced in confluent cultures by incubating the cells in adipogenic induction and maintenance media for 3 days and 1 day, respectively (for media composition please see Tables S3 and 4). Media replacement was repeated 3 times finally leaving the cultures in maintenance medium for 5 days. Cells then were fixed and stained with Oil Red O. Osteogenesis was induced in confluent cultures incubated in osteogenic medium (Table S5) for 10–17 days. Osteogenically differentiated cultures were fixed and stained for accumulated calcium with Alizarin Red. Accumulated calcium was quantified using the Calcium CPC liquicolor kit (Stanbio) as per the manufacturer's instructions. Chondrogenesis was induced in pellet cultures (Johnstone et al., 1998) of 2.5 × 10^5 cells using chondrogenic medium (Table S6). After 21 days of incubation, pellets were either fixed, sectioned and stained with Safranin-O for glycosaminoglycans (GAG) or Papain digested for quantification of the GAG content using 1,9-dimethyl methylene blue (DMMB) as described previously (Enobakhare et al., 1996). GAG values were normalised to cell numbers by measuring the DNA content of the pellet cultures using Pico green assay (Invitrogen) as per the manufacturer's instructions.

Measuring the population doubling times of hBMSC

Passage four hBMSCs were plated on 6-well plates in 3 × 10^4 cell/well density and cultured for 4 days. Following incubation the cells were trypsinised, collected by centrifugation (400 *g* for 5 min at RT) and re-suspended in 1 mL complete culture media. Cell counting was performed in a haemocytometer. Cells were then re-plated on fresh plates as above and steps were repeated until the cultures reached passage six.

Immunofluorescent confocal microscopy

Immunofluorescent confocal microscopy was carried out on cells grown on 96-well μ-Plate plates from Integrated BioDiagnostics (Germany). Cells were fixed in 4% paraformaldehyde (Santa Cruz Biotechnologies, Santa Cruz, CA, USA) for 15 min at room temperature (RT) and washed three times in 1× PBS for 5 min at RT. Cells were permabilized in 1× PBS with 0.1 Triton X-100 for 15 min at RT and washed three times in 1× PBS for 5 min at RT. Specimens were blocked in 1× PBS with 20% normal goat serum and 0.1% Triton X-100 (0.2NGS-PBST) overnight at 4 °C and subsequently incubated in 0.2NGS-PBST containing the anti-phospho-ERK1/2 antibody or normal rabbit serum (negative control) in 1:100 dilution and Alexa Fluor® 647-labelled phalloidin in 1:20 dilution overnight at 4 °C. Cells were washed in 1× PBS 5 times for 5 min at RT and incubated in 0.2NGS-PBST containing the Alexa Fluor 594 goat anti-rabbit IgG (H + L) secondary antibody in 1:200 dilutions for 1 h at 4 °C. Following extensive washing steps, counter staining was performed using 100 μL/well 1× PBS containing 1 μg/mL Hoechs33342 for 1 min at RT. Hoechs33342 was washed out and wells were filled up with 100 μl 1× PBS. Hoechs33342 and AlexaFluor 647-conjugated phalloidin was obtained from Life Technologies Ireland.

Immunoblot

Immunoblot analyses were done as detailed in (Fabian et al., 2009). Primary antibodies used are summarised in Table S2. Species-specific secondary antibodies were purchased from Thermo Scientific. Chemiluminescent signals were detected by FluorChem digital imaging system.

Real-time RT-PCR

Total RNA was isolated using Trizol reagent (Invitrogen) as per the manufacturer's instructions. Concentrations and integrity of RNA isolates were determined by Nanodrop ND-1000 spectrophotometer (NanoDrop Technologies) and Agilent 2100 Bioanalyzer (Agilent), respectively. cDNA synthesis and real-time PCR analysis of samples were performed using High Capacity cDNA Reverse Transcription Kit and TaqMan® Fast Universal PCR Master Mix (Applied Biosystems). Real time PCR reactions were carried out using StepOnePlus thermal cycler (Applied Biosystems). Expression levels were calculated by the delta delta Ct ($\Delta\Delta C_t$) method using Lamin A-specific primers and probes as endogenous control and ROX as passive reference dye. Primers and probes were purchased from Applied Biosystems's gene expression assay library. Used assays are summarised in supplementary Table 7 (Table S7).

ELISA-based DNA binding assay

HIF-1α DNA-binding activity was determined using the HIF-1α specific TRANS-AM kit from Active Motif as per the

manufacturer's instructions. Reactions were quantified by measuring the absorbance of the reaction mixture at 450 nm using Wallac 1420 VICTOR2 microplate reader (Perkin Elmer).

Proximity ligation assay (PLA)

PLA was carried out using the DuoLink labelling system from Sigma according to the manufacturer's instructions. Primary antibodies used were mouse monoclonal anti-HIF-1α (BD; 1:80 dilution) and rabbit monoclonal phospho-specific anti-p42/44 or anti-HIF-1β (Cell Signalling; 1:80 and 1:800 dilutions, respectively). For nuclear counter staining, samples were stained with 0.5 μg/mL Hoechst33342 for 1 min at RT. Amplification was detected using DAPI and TRITC filters of an Olympus IX81 inverted epifluorescent microscope. Pictures were recorded by Volocity software.

Real-time fluorescent correlation spectroscopy (FCS)

FCS measurements were carried out using an FV1000 confocal microscope (Olympus, Germany) equipped with an FCS module (Picoquant, Germany) at λ_{ex} 473 nm and λ_{em} 515–550 nm wavelengths. Emitted fluorescence was focused onto a single photon avalanche diode (Micro Photon Devices, Italy) using a 100 μm pinhole. Fluorescence fluctuations (raw data) were acquired by Symphotime software (Picoquant, Germany). Autocorrelation function ($G(\tau)$) (time-dependent decay) was calculated from fluorescence fluctuation intensity as $G(\tau) = ((\Delta F(\tau) \cdot \Delta F(t + \tau)) / F(t)^2)$, where F(t) is the temporal average of the signal; ΔF(t) is the fluctuation of fluorescence signal defined as deviation from F(t); and $\Delta F(t + \tau)$ is the fluctuation of fluorescence signal at $t + \tau$ deviation from F(t). Measurements were done at 2 randomly selected nuclear positions. Autocorrelation measurements were performed on both spots 6 times for 10 s (Fig. S2). Data with unusual variation or oscillation in the count rates or average photon count rate per second ≤1200 were excluded from further analysis. Autocorrelation curves fitting and the calculation of the average dwell time of the fluorescent species (τD) within the observation volume were carried out as described in (Brazda et al., 2011; Broderick et al., 2012). The diffusion coefficient (D) of the eGFP-tagged HIF-1α was calculated as $D = \omega^2/4\tau_D$. The lateral radius of the observation volume (ω = 0.25 μm) was calculated after calibration using water-dissolved atto488 fluorescent dye (20 nM) (ATTO GmBH, Germany). Diffusion coefficient of the atto488 dye was taken from (Dertinger et al., 2007).

Statistical analysis

Experimental values are expressed as mean value ± SD. For significance analyses, mixed ANOVA was performed. Multiple comparisons were done using Tukey's post-hoc tests with Bonferroni's confidence interval adjustment. P-values ≤0.05 (*), ≤0.01 (**) and ≤0.001 (***) were considered significant, highly significant and extremely significant, respectively.

Results

FGF2 enhances the effects of hypoxia in hBMSCs

To test if the *in vitro* mitogenic pressure interferes with the hypoxic response of hBMSCs, we monitored the proliferation of normoxic and hypoxic cells in the presence or absence of FGF2 by measuring the mean population doubling times (PDT). In accordance with the literature data, FGF2-naïve normoxic cultures ceased to proliferate at passage 5 and 6 showing 99.4 ± 20.9 and 169.3 ± 25.2 h of PDT, respectively, compared to their early passage PDT of 49.5 ± 4.3 h (Fig. 1A). Simultaneously, cells lost their original fibroblast-like phenotype and adopted unusual morphologies towards the late passages (Fig. 1B). In contrast, hBMSCs cultured in FGF2-supplemented media escaped from senescence and preserved the fibroblast phenotype even at late passages. Similarly, FGF2-cultured hBMSCs had significantly reduced PDTs (33.7 ± 3.5, 28.4 ± 2.9 and 43.5 ± 20.4 h at P4, P5 and P6, respectively) compared to the FGF2-naïve cultures over the culturing period observed. Culturing hBMSCs in low oxygen environment had similar effects; cells maintained both constant cell cycle speeds (47.4 ± 0.9, 48.5 ± 4.9 and 55.8 ± 7.4 h at P4, P5 and P6, respectively) and typical hBMSC morphology. Hypoxia-induced proliferation, however, was slightly but significantly slower in the early passage cultures than that of the FGF2-cultured normoxic hBMSCs. Combination of FGF2 and hypoxia had similar effect on hBMSC morphology as the two stimuli alone. Interestingly, FGF2-treatment of hypoxic hBMSCs led to a further reduction of PDTs (28.7 ± 1.6, 32.5 ± 2.9 and 30.8 ± 1.8 h at P4, P5 and P6, respectively) compared to the FGF2-naïve hypoxic cultures. By contrast, hypoxia did not have additive effect on hBMSC proliferation; both FGF2-cultured normoxic and hypoxic cultures had comparable PDTs. To test if FGF2 alters the hypoxic adaptation of hBMSCs at the molecular level, we measured the expression of selected hypoxia-related genes in hBMSCs. We found that the expression of the glucose transporter encoding *SLC2A1* and the intracellular pH regulator carbonic anhydrase IX encoding *CA9* genes were both significantly up-regulated in FGF2-cultured hypoxic hBMSCs compared to their FGF2-naïve counterparts (Figs. 1C-D). The induction of *SLC2A1* and *CA9* were 3- and 10-fold higher, respectively, in FGF2-cultured cells compared to the FGF2-naïve cultures at the end of the 24 hour time course. While the *SLC2A1* relative expression levels were not significantly different in normoxic cells, an approximately 6-fold induction of the basal expression of *CA9* was measured in FGF2-cultured hBMSC cultures over the FGF2-naïve ones under normoxic conditions. Screening the transcriptionally regulated members of the glycolytic genes revealed similar trends in the expression of the triosephosphate isomerase (*TPI1*), glycerol 3-phosphate dehydrogenase (*GPDH*), phosphoglycerate kinase (*PGK1*) and enolase (*ENO*) (Fig. 1E and Fig. S3). The up-regulation was 2 to 3-fold higher in the presence of FGF2 compared to the FGF2-naïve cultures as early as 4–8 h post-exposure. Similar to *CA9*, the up-regulation of the basal gene expression of the *TPI1*, *GPDH*, *PGK1* and *ENO* was also observed in the FGF2-cultured normoxic cells. To a lesser extent, lactate dehydrogenase was also up-regulated in FGF2-cultured hBMSCs but no similar effect was measured in the expression of pyruvate kinase (data not shown). These

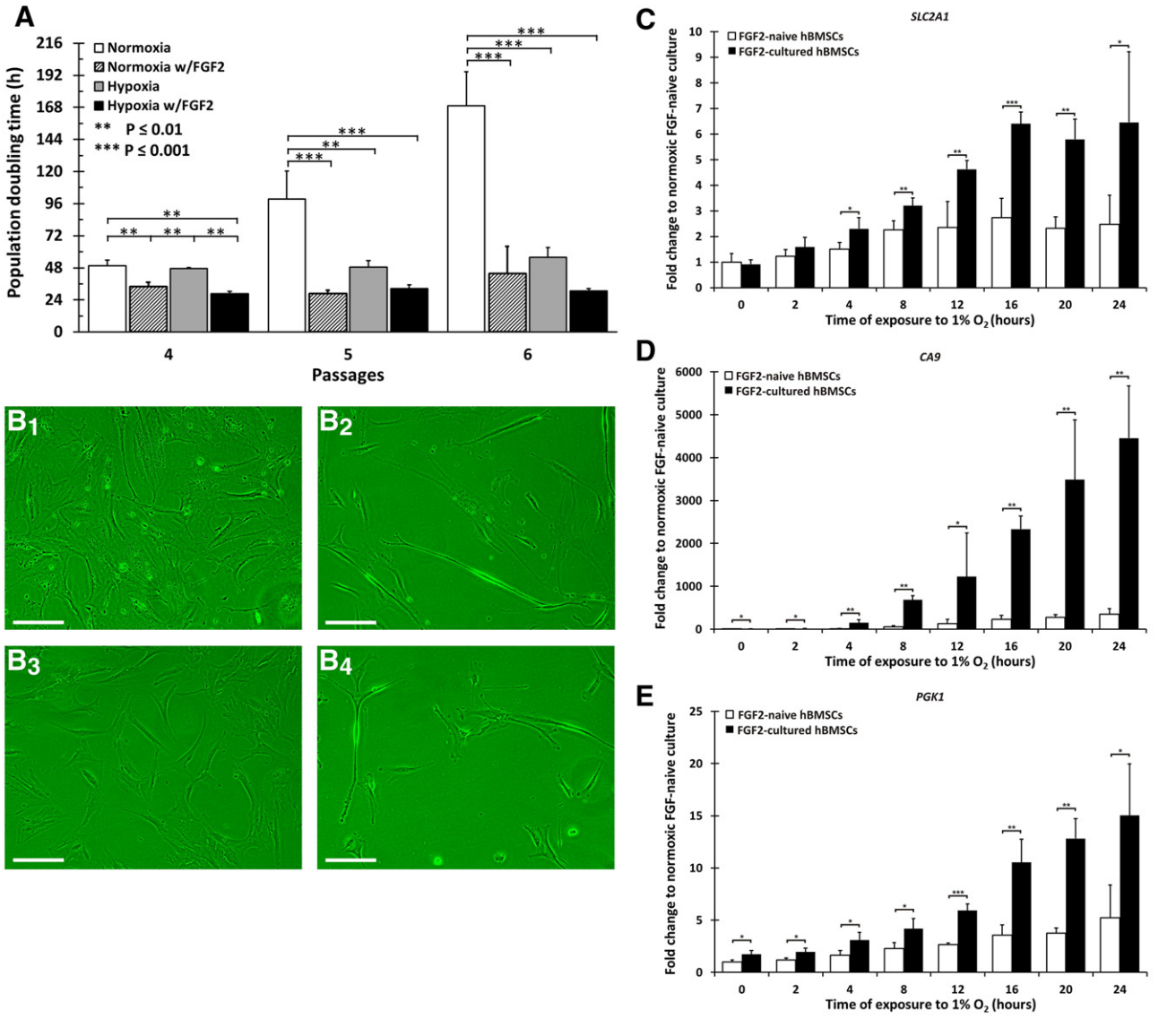

Figure 1 Effects of FGF2 and hypoxia on hBMSC cultures. (A) Population doubling times of hBMSC cultures. Cells were cultured both in the presence (grey and striped bars) or absence (black and white bars) of FGF2 (1 ng/mL) at atmospheric or 2% O_2 levels and population doubling times (PDT) were monitored. PDT values are expressed as mean ± SD (n = 3). (B) Phase-contrast microscopic analysis of cultures kept at atmospheric (B_1 and B_2) or 2% O_2 (B_3 and B_4) in the absence (B_1 and B_3) or presence (B_2 and B_4) of 1 ng/mL FGF2. Images were taken using 10× dry objective lens. Scale bar: 200 μm. (C–E) Expression of hypoxia-related metabolic genes in hBMSC. Cells were cultured in the presence (▮) or absence (▯) of 1 ng/mL FGF2 at atmospheric or 1% O_2 levels for times indicated in the figure. Expression of hypoxia-related metabolic genes (C: glucose transporter [*SLC2A1*]; D: carbonic anhydrase IX [*CA9*]; E: phosphoglycerate kinase [*PGK-1*]) was measured by real time RT-PCR. Gene expression levels are presented as mean fold change to normoxic FGF2-naïve cultures ± SD (n = 3).

Figure 2 FGF2 and hypoxia activates the ERK pathway in hBMSC. (A) Immunoblot analysis of the phosphorylation of ERK1/2 in FGF2-treated hBMSC. (B) Immunofluorescent detection of the nuclear accumulation of p-ERK1/2 (Thr202/Tyr204) in FGF-naïve hBMSC. Nuclei were counterstained using 1 μg/mL Hoechs33342. f-Actin was labelled by AlexaFluor 647-conjugated phalloidin. White arrows indicate positive nuclei. Images were taken using 60× oil immersion objective lens. Scale bar: 10 μm. (C) Immunoblot analysis of the phosphorylation of ERK in hypoxic hBMSCs. Cells were treated with 1 ng/mL FGF2 and 10 μM U0126 as indicated in the figure for 120 min. U0126-treatments preceded the addition of FGF2 by 30 min. (D) Immunoblot analysis of the activation of the ERK pathway in hypoxic hBMSCs. Accumulation of HIF-1α was used as marker of the cellular response to hypoxia. (E) Simultaneous signalling by FGF2 and hypoxia alters the kinetics of the ERK1/2 activation and the HIF-1α accumulation. FGF2-naïve (left panels) and FGF2-cultured (right panels) hBMSCs were exposed to hypoxia (1% O_2) for times indicated in the figure. ERK1/2 phosphorylation and HIF-1α accumulation was monitored by immunoblot. NUCLEOLIN and LAMIN B1 were used as loading controls. (F) Densitometry analysis of Fig. 2E. Loading control-normalised data are expressed as fold change of normoxic cultures.

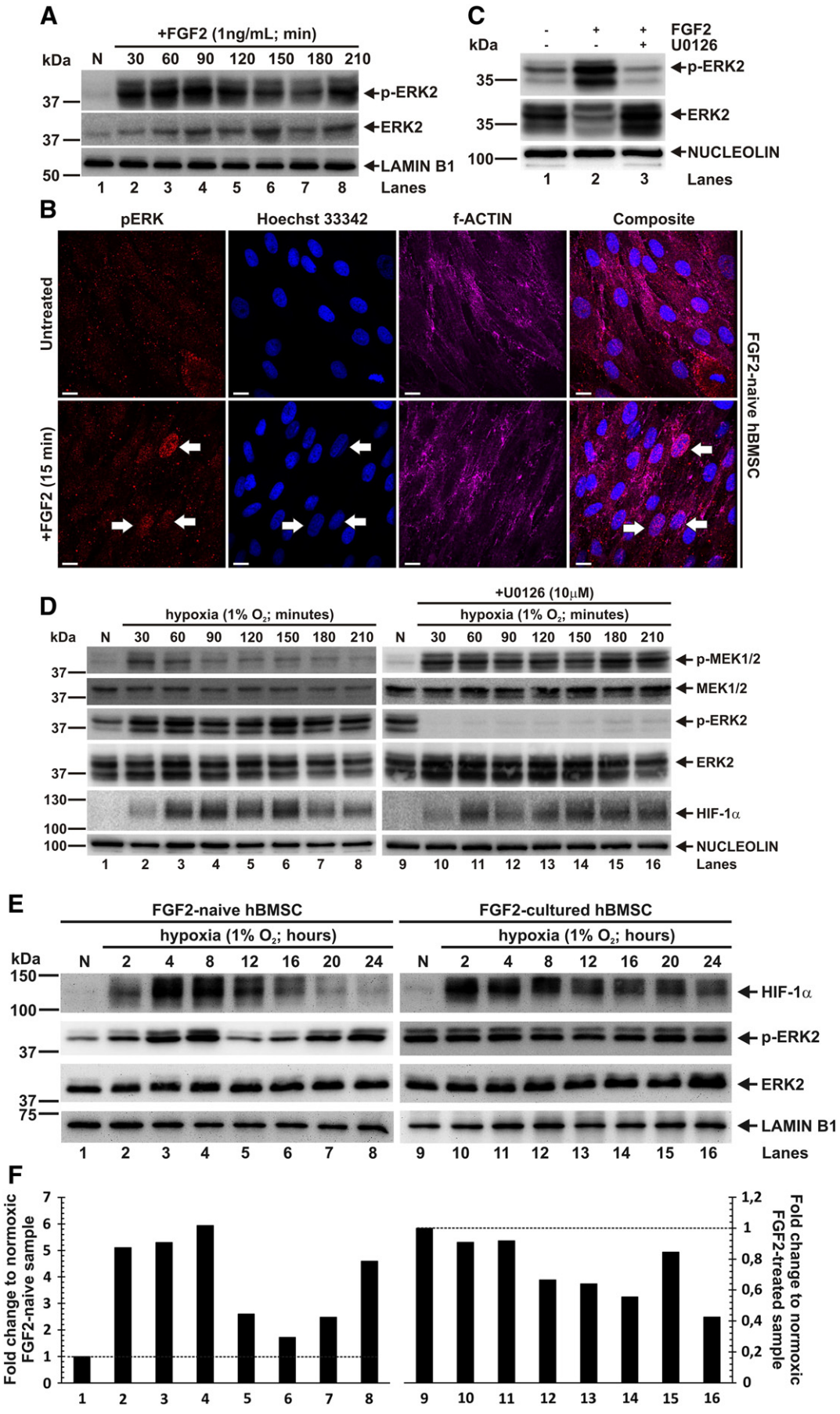
A
+FGF2 (1ng/mL; min)
kDa N 30 60 90 120 150 180 210
37
p-ERK2
37
ERK2
50
LAMIN B1
1 2 3 4 5 6 7 8 Lanes
C
FGF2
U0126
kDa
35
p-ERK2
35
ERK2
100
NUCLEOLIN
1 2 3 Lanes
B
pERK
Hoechst 33342
f-ACTIN
Composite
Untreated
+FGF2 (15 min)
FGF2-naive hBMSC
D
hypoxia (1% O2; minutes)
+U0126 (10μM)
hypoxia (1% O2; minutes)
kDa N 30 60 90 120 150 180 210 N 30 60 90 120 150 180 210
37
p-MEK1/2
37
MEK1/2
37
p-ERK2
37
ERK2
130
100
HIF-1α
100
NUCLEOLIN
1 2 3 4 5 6 7 8 9 10 11 12 13 14 15 16 Lanes
E
FGF2-naive hBMSC
FGF2-cultured hBMSC
hypoxia (1% O2; hours)
hypoxia (1% O2; hours)
kDa N 2 4 8 12 16 20 24 N 2 4 8 12 16 20 24
150
100
HIF-1α
37
p-ERK2
37
ERK2
75
LAMIN B1
1 2 3 4 5 6 7 8 9 10 11 12 13 14 15 16 Lanes
F
Fold change to normoxic FGF2-naive sample
0 1 2 3 4 5 6 7
Fold change to normoxic FGF2-treated sample
0 0,2 0,4 0,6 0,8 1 1,2
1 2 3 4 5 6 7 8 9 10 11 12 13 14 15 16

data indicate that FGF2 enhances the hypoxic response of hBMSCs at the transcriptional level.

Both FGF2 and hypoxia utilise the distal elements of the ERK pathway for immediate signal transduction in hBMSCs

To identify the signalling pathway conveying the FGF2 signal to the transcriptional level in hBMSCs, we tested the phospholipase C gamma 1 (PLCγ1), protein kinase B (PKB/Akt) and extracellular signal-regulated protein kinase (ERK) pathways as the main signalling systems believed to be responsible for transducing the receptor-mediated FGF signals. Immunoblot analysis showed that PLCγ1 was not detectable in hBMSC cultures (Fig. S4A). PKB/Akt was detectable and hypoxia induced activation phosphorylation at Thr308 at 2 h post-exposure indicating the responsiveness of the PKB/Akt system in hBMSCs. However, no activating phosphorylation of PKB/Akt was observed in FGF2-treated normoxic hBMSCs (Fig. S4B). By contrast, immunoblot analysis of ERK1/2 showed rapid phosphorylation at positions Thr202 and Tyr204 of, primarily, ERK2 in a biphasic manner over the first 3 h of the treatment (Fig. 2A). The nuclear accumulation of phosphorylated ERK1/2 occurs within 15 min after the exposure of FGF2-naïve hBMSCs to FGF2 (Fig. 2B). As expected, this effect was blocked by the use of the pharmacological MEK inhibitor U0126 indicating a canonical FGF2-mediated activation of ERKs (Fig. 2C). Similar to FGF2, hypoxia induced biphasic ERK1/2 activation in hBMSCs that could be blocked by U0126 indicating that both FGF2 and hypoxia activate ERK1/2 *via* MEK (Fig. 2D). Unlike ERK1/2, however, MEK phosphorylation at positions Ser217 and 221 was found transient reaching the maximum and then returning to its basal phosphorylation levels at 30 and 90 min post-exposure, respectively. In contrast, phosphorylation of MEK remained sustained in U0126-treated cells, at least, up to 210 min post-exposure. In hypoxic hBMSCs, levels of the hypoxia marker HIF-1α increased 5–6 folds compared to the normoxic cultures by 120–150 min post-exposure. Following the maximum accumulation, HIF-1α levels decreased towards the end of the time course. In contrast, blockade of ERK signalling by MEK inhibition led to reduced rate of HIF-1α accumulation that, however, increased during the 210 min of the hypoxic exposure (Fig. 2D). To test the effects of the simultaneous stimulation of the ERK pathway by FGF2 and hypoxia on the activation of ERK1/2 and HIF-1α, we monitored the ERK1/2 phosphorylation and HIF-1α accumulation over a 24 hour time course. Hypoxia induced ERK1/2 phosphorylation was detectable in both FGF2-naïve and FGF2-cultured cells (Fig. 2E). The dynamics of the ERK1/2 activation, however, was different; FGF-naïve hBMSCs displayed periodicity in the levels of the phosphorylated ERK1/2 over the first 24 h of hypoxia treatment. In contrast, the presence of FGF2 in the culture medium altered the activation dynamics and resulted in a more sustained activation of ERK1/2. HIF-1α was accumulated in both cultures but its stabilisation was delayed and lasted for a shorter time in FGF2-naïve cultures. Our findings indicate that both FGF2 and hypoxia utilise the ERK pathway but the simultaneous presence of the two stimuli alters both the activation dynamics of ERK1/2 and the accumulation of HIF-1α in hypoxic hBMSCs.

FGF2 does not perturb the transcriptional and PHD-mediated regulation of HIF-1α but leads to its co-localisation with activated ERKs in hypoxic hBMSCs

Based on data from cell free, yeast and established cell line model systems, there are different speculations on the link between the ERK and HIF-1α pathways (Bardos et al., 2004; Mylonis et al., 2008; Richard et al., 1999; Sang et al., 2003). To study this question in hBMSCs, we tested if FGF2 alters the oxygen sensitivity of hBMSCs by exposing cells to increasing levels of hypoxia. Cells cultured in normoxic conditions for 3 passages were first exposed to 6% O_2 for 120 min. Following incubation, samples were collected and the oxygen level was further decreased for the remaining cells by 1% for an additional 120 min. Steps were repeated five times and samples were tested for HIF-1α (Figs. 3A–B). We found that HIF-1α was weakly accumulated in both cultures when normoxic cells were exposed to the 6% oxygen environment. However, this initial HIF-1α response became undetectable in cells incubated further at 5% and 4% oxygen levels. Stable accumulation of HIF-1α occurred at 3% oxygen in both FGF2-naïve and FGF2-cultured cells indicating that FGF2 does not elevate the oxygen sensitivity of hBMSCs. The literature data also indicate that in certain conditions HIF-1α can be regulated transcriptionally (Bruning et al., 2011; Fitzpatrick et al., 2011). To study this scenario, we measured the *HIF-1α* expression in hypoxic hBMSCs both in the presence or absence of FGF2. We found a 2–3 fold increase in the basal expression of *HIF-1α* in FGF2-cultured normoxic hBMSCs compared to the FGF2-naïve cells (Fig. 3C). However, FGF2-treatment of the latter cells revealed no immediate induction of *HIF-1α* in the first 48 h of treatment (Fig. 3D). In addition, we also found that the known post-exposure down-regulation of the *HIF-1α* mRNA levels was not affected by FGF2 (Bruning et al., 2011). Together, these data indicate that FGF2 has no direct effects on either the PHD-mediated post-translational or the transcriptional regulation of HIF-1α. To further investigate the relationship between activated ERKs and HIF-1α, we tested if the phosphorylated ERK1/2 binds HIF-1α directly in hypoxic hBMSCs by *in situ* proximity ligation assay (PLA) (Fig. 3E). As positive control, FGF2-naïve hBMSCs were treated with N-(methoxyoxoacetyl)-glycine methyl ester (DMOG) to stabilise HIF-1α in normoxic cells. In DMOG-treated cells, PLA was carried out using HIF-1α and HIF-1β-specific antibodies. As expected, DMOG-treated cells showed robust PLA signals indicating the nuclear formation of HIF-1α/β heterodimers. In untreated normoxic FGF-naïve hBMSC cultures, we could not detect PLA signals using primary antibodies specific to phosphorylated ERK1/2 and HIF-1α. In FGF2-treated hypoxic hBMSCs, however, PLA was positive with strong amplification signals in the majority of FGF2-treated hypoxic hBMSCs at 30 min post-exposure indicating the proximity of the activated ERK1/2 and HIF-1α with the maximum theoretical distance of 30–40 nm. Interestingly, however, although the majority of the phospho-ERK1/2-HIF-1α signals showed nuclear localisation, signals were also detected

with extra nuclear distributions indicating interactions of the two molecules in the cytoplasm as well.

FGF2-treatment results in reduced nuclear diffusion and increased DNA-binding activity of HIF-1α

To further study the impact of the activated ERK1/2 on HIF-1α, we measured the mobility dynamics of HIF-1α using live cell fluorescence correlation spectroscopy (FCS). The advantage of this method is that it provides quantified data on the mobility of the fluorescently tagged target molecule in real-time that directly correlates to the formation of molecular complexes, a critical aspect of the activation of HIF-1α. For FCS analysis, however, the concentration of fluorescent molecules must be within the range of 10–50 nM (maximum 100 nM) to provide high enough signal-to-noise ratios with still detectable fluorescent fluctuations. In addition, cells should be flat enough to make the examined confocal volume stable for the measurements. Unfortunately, due to the limited life span, morphology and poor susceptibility to non-viral transfections of the human bone marrow stromal cultures, we failed to establish an *eGFP-HIF-1α*–carrying hBMSC clone compatible to the absolute requirements of FCS. Instead, considering its physical properties, responsiveness to FGF2 and different dynamics of the ERK activation in the presence or absence of FGF2 under hypoxia, the histologically related U-2 osteosarcoma cell line was chosen to serve as model system (Fig. S5). For FCS, U-2 OS cells were stably transfected with a construct encoding the HIF-1α that was N-terminally tagged with eGFP (U-2 $OS^{eGFP\text{-}HIF\text{-}1\alpha}$) and clones with eGFP-HIF-1α levels most appropriate for FCS was selected ($U9^{eGFP\text{-}HIF\text{-}1\alpha}$). $U9^{eGFP\text{-}HIF\text{-}1\alpha}$ cells were exposed to 1% O_2 in the presence or absence of FGF2 and U0126 and subjected to FCS. In FGF2-naïve cells, significant reduction in the diffusion coefficient ($D^{eGFP\text{-}HIF\text{-}1\alpha}$) of HIF-1α was first detected at 4 h post-exposure in the nucleus when approximately 5% and 10% of the cells showed diffusion coefficients of 21.45 ± 0.7 and 8.06 ± 4.19 μm²/s, respectively (Figs. 4A–B and Table S1). However, in the

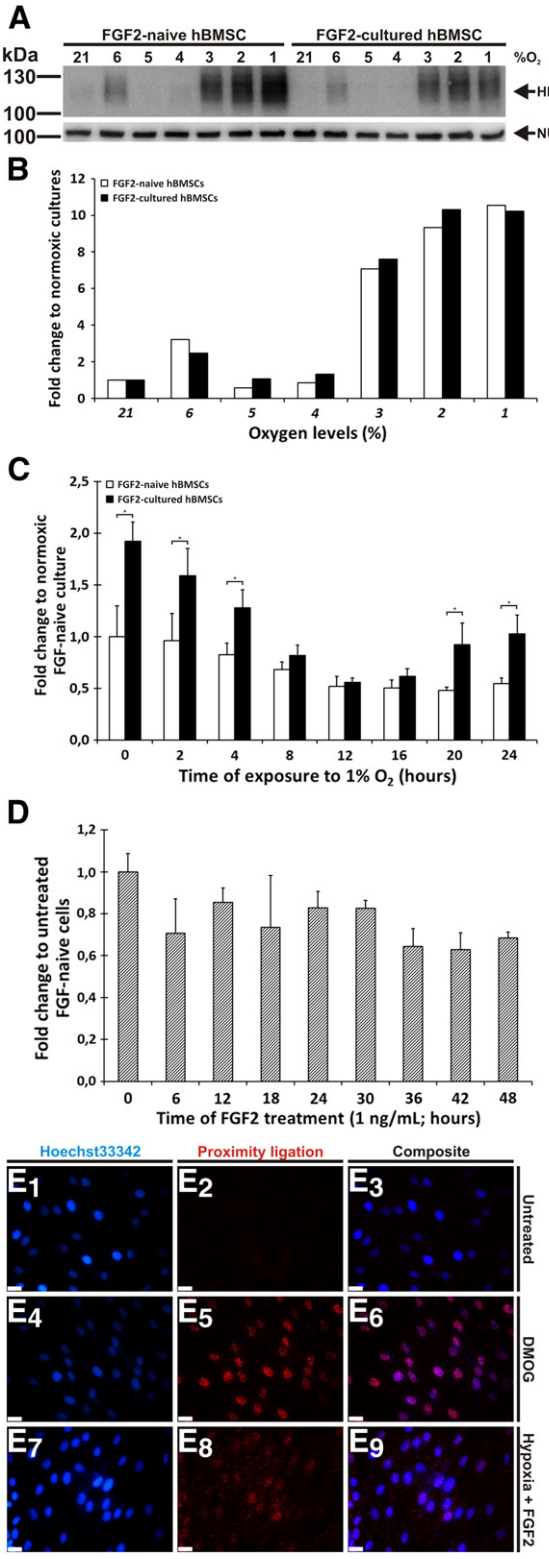

Figure 3 Interaction between the FGF2-activated MAPK pathway and HIF-1α in hypoxic hBMSCs. (A) FGF2 does not perturb the sensitivity of hBMSCs to oxygen. FGF2-naïve and FGF2-cultured hBMSCs were maintained under normoxic conditions or exposed to various oxygen levels as indicated in the figure. Whole cell lysates were tested for HIF-1α accumulation by immunoblot. Nucleolin was used as loading control. (B) Densitometry analysis of Fig. 3A. Loading control-normalised data of FGF2-naive (▯) and FGF2-cultured (▮) hBMSCs are expressed as fold change of normoxic cultures. (C–D) FGF2 induces *HIF-1α* basal expression indirectly without disturbing transcriptional feedback regulation. (C) Analysis of HIF-1α mRNA levels of FGF2-naive (▯) and FGF2-cultured (▮) hBMSCs exposed to hypoxia. *HIF-1α* mRNA levels were measured by real time RT-PCR. Data are expressed as mean fold change to FGF2-naïve normoxic cultures ± SD (n = 3). (D) Analysis of *HIF-1α* mRNA levels of FGF2-naïve cells treated with FGF2 as indicated in the figure. *HIF-1α* mRNA levels were measured by real time RT-PCR. Data are expressed as mean fold change to FGF2-naïve normoxic cultures ± SD (n = 3). (E) HIF-1α and phospho-ERK1/2 co-localise in hypoxic hBMSCs. Proximity ligation assay (PLA) was carried out in untreated normoxic (E_1–E_3) and FGF2-treated hypoxic (E_7–E_9) FGF-naïve hBMSCs at 30 min post-exposure using phospho-specific ERK1/2 and HIF-1α-specific primary antibodies. As positive control, stabilisation and dimerization of HIF-1α with HIF-1β was induced with 1 mM DMOG for 60 min (E_4–E_6). PLA was carried out in DMOG-treated FGF-naïve cells using HIF-1α- and HIF-1β-specific primary antibodies. Images were taken using 40× water immersion objective lens. Scale bar: 24 μm.

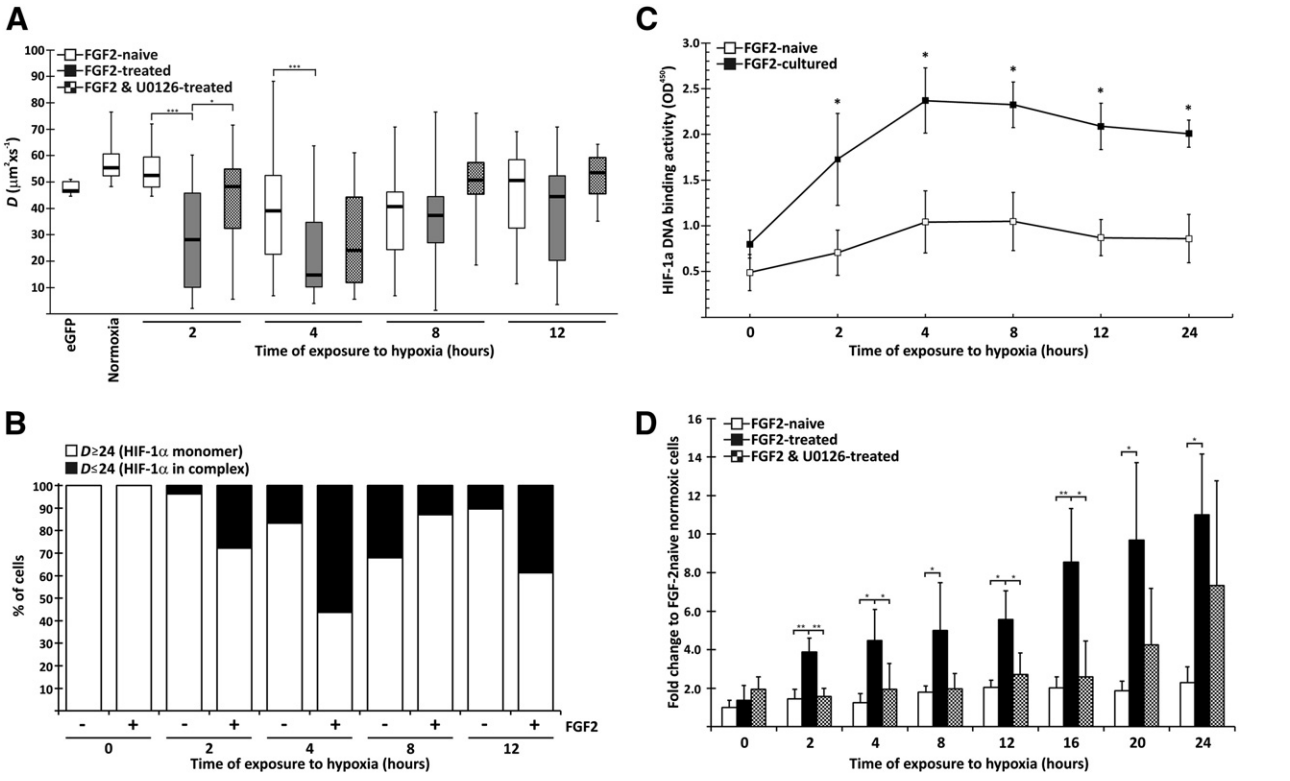

Figure 4 FGF2 enhances HIF-1α activity in hypoxic hBMSCs. (A) FGF2 reduces nuclear diffusion of HIF-1α and facilitates the formation of multiprotein complexes. Live cell fluorescence correlation spectroscopy (FCS) of eGFP-tagged HIF-1α was carried out using FGF2-naïve (□), FGF2-treated (■) and FGF2 + U0126-treated (chequered boxes) U-2 osteosarcoma (U-2 OS) cells from 3 independent experiments. Data are presented as median (bold line) with the first and third quartiles (top and bottom of boxes) and minimum/maximum values (negative/positive bars). (B) FGF2 increases the proportion of cells with complexed HIF-1α. Using molecular diffusion data, the molecular mass of the HIF-1α species were calculated (Table S1). Data were clustered according to the molecular masses representing either monomeric (□) or complexed (■) HIF-1α species. (C) FGF2 enhances *in vitro* HIF-1α DNA-binding activity of nuclear lysates of hBMSC. Normoxic and hypoxic FGF-naive (□) and FGF2-cultured (■) hBMSCs were screened for HIF-1α DNA binding activity at time points indicated in the figure. Data are expressed as fold change to values measured in normoxic cultures ± SD (n = 3). (D) FGF2 enhances HIF-1α-regulated *VEGF-A* induction in hypoxic hBMSCs. *VEGF-a* mRNA levels were measured by real time RT-PCR in FGF2-naïve (□), FGF2-treated (■) and FGF2 + U0126-treated (chequered boxes) hBMSCs exposed to hypoxia for times indicated in the figure. Data are expressed as mean fold change to FGF2-naïve normoxic cultures ± SD (n = 3).

majority of the examined cells (83.3%) $D^{eGFP\text{-}HIF\text{-}1\alpha}$ remained comparable to that of the normoxic cells (Fig. 4B). The maximum reduction of $D^{eGFP\text{-}HIF\text{-}1\alpha}$ was observed at 8 h post-exposure (Fig. 4A) when approximately one-third of the cells showed slow or very slow components with the mean $D^{eGFP\text{-}HIF\text{-}1\alpha}$ = 10.68 ± 3.75 μm²/s while 2/3 of the cells were still closer to the normoxic counterparts ($D^{eGFP\text{-}HIF\text{-}1\alpha}$ = 45.79 ± 9.95 μm²/s) (Fig. 4B and Table S1). Reduction of the HIF-1α diffusion was resolved by 12 h post-exposure when 80% of the cells had fast components and only 10% of the cells retained slow or very slow HIF-1α species (Fig. 4B). In contrast, FGF2-treated hypoxic cells showed prompt and significant reduction of $D^{eGFP\text{-}HIF\text{-}1\alpha}$ as early as 2 h post-treatment (Fig. 4A). The proportion of the cells with fast components ($D^{eGFP\text{-}HIF\text{-}1\alpha}$ = 45.11 ± 12.8 μm²/s) was reduced to ~70% and approximately 25% of the cells showed slow diffusion components with $D^{eGFP\text{-}HIF\text{-}1\alpha}$ = 9.15 ± 4.56 μm²/s (Fig. 4B and Table S1). This was further increased by 4 h post-treatment when 58% of the cells showed slow species ($D^{eGFP\text{-}HIF\text{-}1\alpha}$ = 9.03 ± 4.48 μm²/s) (Fig. 4B). Unlike FGF-naïve cells, however, the maximal reduction of HIF-1α diffusion was resolved between 4 and 8 h post-exposure (Fig. 4A). The proportion of the cells with fast species of HIF-1α was increased to 75% and only 10% displayed very slow diffusing forms ($D^{eGFP\text{-}HIF\text{-}1\alpha}$ = 44.57 ± 10.7 and 9.44 ± 4.98 μm²/s, respectively) by 8 h post-exposure (Fig. 4B and Table S1). We found no significant difference between the nuclear diffusion of HIF-1α in FGF2-naïve and FGF2-treated cells at 30, 60 and 90 min post-exposure (data not shown). In addition, we did not detect any change in HIF-1α diffusion within the cytoplasm irrespectively of the FGF2 status of the cells (data not shown). Pre-treatment of the FGF2-treated cells with U0126 reversed the diffusion rate of eGFP-HIF-1α to similar levels to that of the FGF2-naïve cells at 2, 8 and 12 h post-exposure with mean $D^{eGFP\text{-}HIF\text{-}1\alpha}$ values of 42.7 ± 17.4, 51.7 ± 12.0 and 52.0 ± 7.9 μm²/s, respectively (Fig. 4A). Interestingly, at 4 h post-exposure, we detected slow diffusion species of eGFP-HIF1α with the diffusion rate of 28.0 ± 17.6 μm²/s. It is noteworthy, however, that in U0126-treated cultures,

we detected autocorrelation curves with suitably high signal-to-noise ratio in only 22% of the examined cells and this phenomenon was particularly pronounced at 2 and 4 h post-exposure. Using our FCS data combined with the reference diffusion coefficient of the 27 kDa eGFP and the assumption of the approximately spherical shape of the molecular objects in question, we also calculated the molecular mass of eGFP-HIF-1α-containing molecular structures (Table S1). Our calculations showed dramatic differences in the molecular mass of HIF-1α-containing complexes in the presence or absence of FGF2. In FGF2-treated cells, significantly higher molecular masses (738.4 MDa) were calculated as early as 2 h post-exposure compared to the FGF2-naïve cells. Furthermore, HIF-1α species were more homogenous and the frequency of HIF-1α-containing mega Dalton complexes was higher in the presence of FGF2 (Table S1). To test if the alterations in its diffusion correlate with the DNA-binding activity of HIF-1α in hBMSCs as well, we measured the amount of HIF-1α bound to its consensus sequence in the promoter of the *erythropoietin* gene using nuclear lysates of both FGF2-naïve and FGF2-treated hBMSC cultures (Fig. 4C). In normoxic conditions, comparable amount of HIF-1α activity was measured in both cultures that steadily increased in hypoxia to the maximum DNA-binding activity at 8 h post-exposure. This was then followed by moderate decrease in DNA-bound HIF-1α levels. In FGF2-cultured cells, however, the amount of the DNA-bound form of HIF-1α was increased more robustly showing a 3–4 fold increase compared to the FGF2-naïve cells over the first 2 h of the hypoxic exposure. Peak HIF-1α DNA-binding activity was observed between 4 and 8 h post-treatment followed by a slight decrease between 8 and 24 h post-exposure. The difference between the FGF2-naïve and treated cultures, however, was maintained over the first 24 h of the hypoxic exposure. To confirm these data in a physiologically more relevant context, we monitored the expression of the vascular endothelial growth factor-alpha (*VEGF-A*) gene, a known HIF-1α target, in hypoxic hBMSCs in the presence or absence of FGF2 and U0126 (Fig. 4D). FGF2-naïve cultures increased *VEGF-A* expression very moderately over the first 24 h of hypoxic exposure showing an approximately 2-fold maximum induction after 12 h post exposure. In contrast, FGF2-cultured hBMSCs responded more promptly to hypoxia by inducing *VEGF-A* as early as 2 h post-exposure steadily increasing mRNA levels over the first 24 h of the hypoxic exposure. The use of U0126 reversed this response similarly to that of the FGF2-naïve cultures and this effect was particularly pronounced at the early time points up to 16 h post-exposure.

Discussion

In vitro, hBMSCs are capable of differentiating into a variety of cell types including osteo-, chondro- and adipocytes (Pittenger et al., 1999). This fuelled the idea of their use for regenerative cellular therapy of a wide range of human pathologies including those that affect tissues of the skeletal system (Bianco et al., 2001). Although the related pathological conditions may have distinct pathogenesis, hypoxia is one of the few known pathological factors. hBMSCs naturally reside in a poorly oxygenised microenvironment making them particularly attractive for cellular therapy of conditions either affecting poorly vascularised tissues *e.g.* cartilage or related to pathological forms of hypoxia like the metabolic hypoxia in chronic inflammatory diseases like osteoarthritis (Chow et al., 2001; Tondevold et al., 1979).

During their *ex vivo* expansion, donor cells are kept in conditions fundamentally different from their natural niche in terms of the oxygen levels or increased mitogenic pressure. The impact of the *ex vivo* expansion on the hypoxic adaptation of hBMSCs, however, has remained unexplored. Here, we found that, *in vitro*, the hypoxia-adaptive responses are enhanced in the presence of FGF2 including the robust induction of genes encoding glycolytic enzymes, intracellular homeostasis regulators, glucose transporters or VEGF, suggesting that FGF2-treated hBMSCs may adapt to the hypoxic milieu more efficiently.

As FGFs are primarily considered mitogenic factors, our data also indicate the direct link between mechanisms controlling proliferation and hypoxic adaptation of hBMSCs. Indeed, we identified the ERK pathway to convey FGF2 signals. Interestingly, similar to established cell lines, we found that hypoxia also activates the distal elements of the ERK pathway in hBMSCs and the dynamics of this activation is similar to that of the FGF2 questioning the mechanism of action of the FGF2 on the hypoxic response in hBMSCs (Minet et al., 2000). The more sustained ERK activation during the co-stimulation by FGF2 and hypoxia compared to the dynamics observed upon the activation by only a single stimulus may provide an explanation for this question. Indeed, differential dynamics of the ERK pathway may lead to distinct biological effects as was shown in other model systems (Yoon and Deisboeck, 2009). In the case of hBMSCs, the simultaneous presence of the two stimuli led to higher cell numbers during their *in vitro* expansion. Since we found no statistical difference in the number of the colony forming unit fibroblasts in hBMSC cultures treated with any combination of FGF2 and hypoxia/normoxia (data not shown), we concluded that the higher yield in cell numbers are primarily due to upregulation of the proliferation.

Although the relationship between HIF-1 and the ERK pathways has already been reported in established cell lines, the nature of this interaction remained obscure as reports indicated both direct and indirect effects of ERK activation on HIF-1 activity (Bilton and Booker, 2003; Mylonis et al., 2008; Sang et al., 2003). For the first time, we approached this question using live cell fluorescence correlation spectroscopy and measured the mobility dynamics of the eGFP-tagged HIF-1α in the context of the FGF2-induced ERK activation. As a result, we observed interesting differences in the diffusion coefficients of eGFP-HIF-1α ($D^{eGFP\text{-}HIF\text{-}1\alpha}$) comparing both normoxic-hypoxic as well as FGF2-naïve and FGF2-treated cells. Despite the Stokes–Einstein relation that predicts eGFP-tagged molecules diffusing more slowly than the standalone eGFP, we found the $D^{eGFP\text{-}HIF\text{-}1\alpha}$ increased by a factor of 1.3 over the diffusion coefficients of eGFP (D^{eGFP}) in normoxic cells. D^{eGFP} was calculated using experimental curves fitted to the one component free diffusion model that resulted in D^{eGFP} comparable to literature values (Jeyasekharan et al., 2010). This led us to speculate that the elevated $D^{eGFP\text{-}HIF\text{-}1\alpha}$ measured in normoxic cells may represent active transport mechanisms rather than Brownian motion. Indeed, recent reports suggested that the VHL protein

interacts with microtubules through kinesin-2 (Carbonaro et al., 2012). Under hypoxia, the elevated basal $D^{eGFP\text{-}HIF\text{-}1\alpha}$ was significantly reduced. Theoretically, reduction of the nucleoplasmic mobility could have accounted for the formation of protein complexes, molecular crowding, transient intermolecular interactions or obstructions by immobile nuclear structures (Bancaud et al., 2009; Fritsch and Langowski, 2011). The latter one is believed to result in very slow species (0.1–2 $\mu m^2/s$) but this was not observed in our FGF2-naïve hypoxic cells (Jeyasekharan et al., 2010). Moreover, since our data fitted the one component free diffusion model with residual fit close to zero (Fig. S2), we excluded both molecular obstruction and crowding and speculate that the most likely cause of the $D^{eGFP\text{-}HIF\text{-}1\alpha}$ reduction is complex formation. Using our FCS data, we also calculated the molecular masses of the eGFP-HIF-1α-containing structures. These calculations suggest that HIF-1α may be in different molecular complexes in the nucleus depending on the activation status of the ERK pathway. Our data indicate that the activation of the ERK pathway not only contributes to the temporal regulation of the formation of HIF-1α-containing nuclear complexes but also to the molecular compositions of the same resulting in significant impact on the regulatory functions of HIF-1α and, consequently, the adaptive response to hypoxia (Fig. 5) (Sang et al., 2003; Semenza, 2007; Wotzlaw et al., 2007).

In vitro, the hypoxic exposure of hBMSCs positively influences their differentiation capacity, metabolism or senescence (Dos Santos et al., 2010; Grayson et al., 2007; Jin et al., 2010). In our current study, we identified the FGF2-mediated activation of the ERK pathway as a potential regulator of the HIF-1α-mediated hypoxic response of hBMSCs.

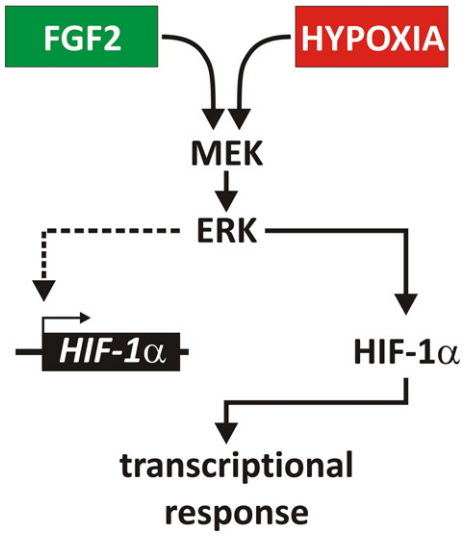

Figure 5 ERK pathway has dual effect on the transcriptional regulation of the hypoxia response in hBMSCs. Our data indicate that FGF2 and hypoxia both activate the ERK pathway. In short term, this activation facilitates the complex formation and DNA binding of the stabilised HIF-1α and represents a direct physical link between the ERK- and HIF-1α-mediated molecular events (continuous line). Long term FGF2 treatment, however, has an additional but indirect effect on the HIF-1 machinery by the elevation of the basal expression of *HIF-1α* gene in normoxic cells (dashed line).

However, our finding that the ERK pathway is utilised by both stimuli raises the question if hypoxia has effects on hBMSCs similar to those of FGF2 that, while apparently not interfering with the differentiation capacity of hBMSCs *in vitro*, was shown to have an adverse effect on the hBMSC-mediated ectopic formation of the hematopoetic microenvironment *in vivo* (Sacchetti et al., 2007). Although FGF2 and hypoxia appeared to be synergistic on the proliferation of our hBMSCs *in vitro*, the functionality of the FGF2-cultured hypoxic hBMSCs needs to be confirmed in more appropriate *in vivo* models. Understanding the underlying regulatory mechanisms of the two stimuli, however, may contribute to the better determination of the culturing conditions for hBMSCs.

Conclusion

Our observations strongly indicate that the activation status of the ERK pathway has an important role in the hypoxic response of hBMSCs. As we found the ERK pathway to be the immediately responding signalling machinery to the mitotic stimulus of FGF2 and that the donor-to-donor heterogeneity in terms of proliferation and differentiation capacity is a well-known feature of the *in vitro* maintained hBMSC cultures, we hypothesise that the different proportions of the proliferating species in any individual bone marrow aspirates may be a critical factor to the post-transplantation fate of the hBMSC populations in the hypo- or anoxic milieu. Similarly, the impact of the *ex vivo* manipulations on the status of the ERK pathway may also be important when cells are considered to be used in cellular therapy of medical situations with different levels of hypoxia.

Supplementary data to this article can be found online at http://dx.doi.org/10.1016/j.scr.2014.02.007.

Acknowledgments

The authors wish to thank professor Noel Lowndes for the wild type U-2 OS and Dr. Chiara Saladino for the $U9^{eGFP\text{-}HIF\text{-}1\alpha}$ cells and Andrea Keogh for the technical assistance.

References

Bancaud, A., Huet, S., Daigle, N., Mozziconacci, J., Beaudouin, J., Ellenberg, J., 2009. Molecular crowding affects diffusion and binding of nuclear proteins in heterochromatin and reveals the fractal organization of chromatin. Embo J. 28, 3785–3798.

Bardos, J.I., Chau, N.M., Ashcroft, M., 2004. Growth factor-mediated induction of HDM2 positively regulates hypoxia-inducible factor 1alpha expression. Mol. Cell. Biol. 24, 2905–2914.

Beenken, A., Mohammadi, M., 2009. The FGF family: biology, pathophysiology and therapy. Nat. Rev. Drug Discov. 8, 235–253.

Bianco, P., Riminucci, M., Gronthos, S., Robey, P.G., 2001. Bone marrow stromal stem cells: nature, biology, and potential applications. Stem Cells 19, 180–192.

Bilton, R.L., Booker, G.W., 2003. The subtle side to hypoxia inducible factor (HIFalpha) regulation. Eur. J. Biochem. 270, 791–798.

Brazda, P., Szekeres, T., Bravics, B., Toth, K., Vamosi, G., Nagy, L., 2011. Live-cell fluorescence correlation spectroscopy dissects the role of coregulator exchange and chromatin binding in retinoic acid receptor mobility. J. Cell Sci. 124, 3631–3642.

Broderick, R., Ramadurai, S., Toth, K., Togashi, D.M., Ryder, A.G., Langowski, J., Nasheuer, H.P., 2012. Cell cycle-dependent mobility of Cdc45 determined *in vivo* by fluorescence correlation spectroscopy. PLoS One 7, e35537.

Bruning, U., Cerone, L., Neufeld, Z., Fitzpatrick, S.F., Cheong, A., Scholz, C.C., Simpson, D.A., Leonard, M.O., Tambuwala, M.M., Cummins, E.P., et al., 2011. MicroRNA-155 promotes resolution of hypoxia-inducible factor 1alpha activity during prolonged hypoxia. Mol. Cell. Biol. 31, 4087–4096.

Carbonaro, M., Escuin, D., O'Brate, A., Thadani-Mulero, M., Giannakakou, P., 2012. Microtubules regulate hypoxia-inducible factor-1alpha protein trafficking and activity: implications for taxane therapy. J. Biol. Chem. 287, 11859–11869.

Chan, D.A., Sutphin, P.D., Denko, N.C., Giaccia, A.J., 2002. Role of prolyl hydroxylation in oncogenically stabilized hypoxia-inducible factor-1alpha. J. Biol. Chem. 277, 40112–40117.

Chen, Y., Li, X., Eswarakumar, V.P., Seger, R., Lonai, P., 2000. Fibroblast growth factor (FGF) signaling through PI 3-kinase and Akt/PKB is required for embryoid body differentiation. Oncogene 19, 3750–3756.

Chen, S.L., Fang, W.W., Ye, F., Liu, Y.H., Qian, J., Shan, S.J., Zhang, J.J., Chunhua, R.Z., Liao, L.M., Lin, S., et al., 2004. Effect on left ventricular function of intracoronary transplantation of autologous bone marrow mesenchymal stem cell in patients with acute myocardial infarction. Am. J. Cardiol. 94, 92–95.

Chikazu, D., Hakeda, Y., Ogata, N., Nemoto, K., Itabashi, A., Takato, T., Kumegawa, M., Nakamura, K., Kawaguchi, H., 2000. Fibroblast growth factor (FGF)-2 directly stimulates mature osteoclast function through activation of FGF receptor 1 and p42/p44 MAP kinase. J. Biol. Chem. 275, 31444–31450.

Chow, D.C., Wenning, L.A., Miller, W.M., Papoutsakis, E.T., 2001. Modeling pO(2) distributions in the bone marrow hematopoietic compartment. I. Krogh's model. Biophys. J. 81, 675–684.

Cuevas, P., Carceller, F., Ortega, S., Zazo, M., Nieto, I., Gimenez-Gallego, G., 1991. Hypotensive activity of fibroblast growth factor. Science 254, 1208–1210.

Dertinger, T., Pacheco, V., von der Hocht, I., Hartmann, R., Gregor, I., Enderlein, J., 2007. Two-focus fluorescence correlation spectroscopy: a new tool for accurate and absolute diffusion measurements. Chemphyschem: Eur. J. Chem. Phys. Phys. Chem. 8, 433–443.

Dominici, M., Le Blanc, K., Mueller, I., Slaper-Cortenbach, I., Marini, F., Krause, D., Deans, R., Keating, A., Prockop, D., Horwitz, E., 2006. Minimal criteria for defining multipotent mesenchymal stromal cells. The International Society for Cellular Therapy position statement. Cytotherapy 8, 315–317.

Dos Santos, F., Andrade, P.Z., Boura, J.S., Abecasis, M.M., da Silva, C.L., Cabral, J.M., 2010. *Ex vivo* expansion of human mesenchymal stem cells: a more effective cell proliferation kinetics and metabolism under hypoxia. J. Cell. Physiol. 223, 27–35.

Eisemann, A., Ahn, J.A., Graziani, G., Tronick, S.R., Ron, D., 1991. Alternative splicing generates at least five different isoforms of the human basic-FGF receptor. Oncogene 6, 1195–1202.

Enobakhare, B.O., Bader, D.L., Lee, D.A., 1996. Quantification of sulfated glycosaminoglycans in chondrocyte/alginate cultures, by use of 1,9-dimethylmethylene blue. Anal. Biochem. 243, 189–191.

Fabian, Z., O'Brien, P., Pajecka, K., Fearnhead, H.O., 2009. TPCK-induced apoptosis and labelling of the largest subunit of RNA polymerase II in Jurkat cells. Apoptosis 14, 1154–1164.

Fitzpatrick, S.F., Tambuwala, M.M., Bruning, U., Schaible, B., Scholz, C.C., Byrne, A., O'Connor, A., Gallagher, W.M., Lenihan, C.R., Garvey, J.F., et al., 2011. An intact canonical NF-kappaB pathway is required for inflammatory gene expression in response to hypoxia. J. Immunol. 186, 1091–1096.

Fritsch, C.C., Langowski, J., 2011. Chromosome dynamics, molecular crowding, and diffusion in the interphase cell nucleus: a Monte Carlo lattice simulation study. Chromosom. Res.: Int. J. Mol., Supramol. Evol. Asp. Chromosom. Biol. 19, 63–81.

Fulgham, D.L., Widhalm, S.R., Martin, S., Coffin, J.D., 1999. FGF-2 dependent angiogenesis is a latent phenotype in basic fibroblast growth factor transgenic mice. Endothelium 6, 185–195.

Grayson, W.L., Zhao, F., Bunnell, B., Ma, T., 2007. Hypoxia enhances proliferation and tissue formation of human mesenchymal stem cells. Biochem. Biophys. Res. Commun. 358, 948–953.

Ivan, M., Haberberger, T., Gervasi, D.C., Michelson, K.S., Gunzler, V., Kondo, K., Yang, H., Sorokina, I., Conaway, R.C., Conaway, J.W., et al., 2002. Biochemical purification and pharmacological inhibition of a mammalian prolyl hydroxylase acting on hypoxia-inducible factor. Proc. Natl. Acad. Sci. U. S. A. 99, 13459–13464.

Jeyasekharan, A.D., Ayoub, N., Mahen, R., Ries, J., Esposito, A., Rajendra, E., Hattori, H., Kulkarni, R.P., Venkitaraman, A.R., 2010. DNA damage regulates the mobility of Brca2 within the nucleoplasm of living cells. Proc. Natl. Acad. Sci. U. S. A. 107, 21937–21942.

Jin, Y., Kato, T., Furu, M., Nasu, A., Kajita, Y., Mitsui, H., Ueda, M., Aoyama, T., Nakayama, T., Nakamura, T., et al., 2010. Mesenchymal stem cells cultured under hypoxia escape from senescence *via* down-regulation of p16 and extracellular signal regulated kinase. Biochem. Biophys. Res. Commun. 391, 1471–1476.

Johnson, D.E., Lu, J., Chen, H., Werner, S., Williams, L.T., 1991. The human fibroblast growth factor receptor genes: a common structural arrangement underlies the mechanisms for generating receptor forms that differ in their third immunoglobulin domain. Mol. Cell. Biol. 11, 4627–4634.

Johnstone, B., Hering, T.M., Caplan, A.I., Goldberg, V.M., Yoo, J.U., 1998. *In vitro* chondrogenesis of bone marrow-derived mesenchymal progenitor cells. Exp. Cell Res. 238, 265–272.

Kanichai, M., Ferguson, D., Prendergast, P.J., Campbell, V.A., 2008. Hypoxia promotes chondrogenesis in rat mesenchymal stem cells: a role for AKT and hypoxia-inducible factor (HIF)-1alpha. J. Cell. Physiol. 216, 708–715.

Macmillan, M.L., Blazar, B.R., DeFor, T.E., Wagner, J.E., 2009. Transplantation of ex-vivo culture-expanded parental haploidentical mesenchymal stem cells to promote engraftment in pediatric recipients of unrelated donor umbilical cord blood: results of a phase I–II clinical trial. Bone Marrow Transplant. 43, 447–454.

Majmundar, A.J., Wong, W.J., Simon, M.C., 2010. Hypoxia-inducible factors and the response to hypoxic stress. Mol. Cell 40, 294–309.

Martin, I., Muraglia, A., Campanile, G., Cancedda, R., Quarto, R., 1997. Fibroblast growth factor-2 supports *ex vivo* expansion and maintenance of osteogenic precursors from human bone marrow. Endocrinology 138, 4456–4462.

Masson, N., Willam, C., Maxwell, P.H., Pugh, C.W., Ratcliffe, P.J., 2001. Independent function of two destruction domains in hypoxia-inducible factor-alpha chains activated by prolyl hydroxylation. Embo J. 20, 5197–5206.

Mazzini, L., Ferrero, I., Luparello, V., Rustichelli, D., Gunetti, M., Mareschi, K., Testa, L., Stecco, A., Tarletti, R., Miglioretti, M., et al., 2010. Mesenchymal stem cell transplantation in amyotrophic lateral sclerosis: a phase I clinical trial. Exp. Neurol. 223, 229–237.

Miller, D.L., Ortega, S., Bashayan, O., Basch, R., Basilico, C., 2000. Compensation by fibroblast growth factor 1 (FGF1) does not account for the mild phenotypic defects observed in FGF2 null mice. Mol. Cell. Biol. 20, 2260–2268.

Minet, E., Arnould, T., Michel, G., Roland, I., Mottet, D., Raes, M., Remacle, J., Michiels, C., 2000. ERK activation upon hypoxia: involvement in HIF-1 activation. FEBS Lett. 468, 53–58.

Mohammadi, M., Olsen, S.K., Ibrahimi, O.A., 2005. Structural basis for fibroblast growth factor receptor activation. Cytokine Growth Factor Rev. 16, 107–137.

Mylonis, I., Chachami, G., Paraskeva, E., Simos, G., 2008. Atypical CRM1-dependent nuclear export signal mediates regulation of

hypoxia-inducible factor-1alpha by MAPK. J. Biol. Chem. 283, 27620–27627.

Park, S.Y., Barron, E., Suh, P.G., Ryu, S.H., Kay, E.P., 1999. FGF-2 facilitates binding of SH3 domain of PLC-gamma1 to vinculin and SH2 domains to FGF receptor in corneal endothelial cells. Mol. Vis. 5, 18.

Perez-Simon, J.A., Lopez-Villar, O., Andreu, E.J., Rifon, J., Muntion, S., Campelo, M.D., Sanchez-Guijo, F.M., Martinez, C., Valcarcel, D., Canizo, C.D., 2011. Mesenchymal stem cells expanded *in vitro* with human serum for the treatment of acute and chronic graft-versus-host disease: results of a phase I/II clinical trial. Haematologica 96, 1072–1076.

Pittenger, M.F., Mackay, A.M., Beck, S.C., Jaiswal, R.K., Douglas, R., Mosca, J.D., Moorman, M.A., Simonetti, D.W., Craig, S., Marshak, D.R., 1999. Multilineage potential of adult human mesenchymal stem cells. Science 284, 143–147.

Richard, D.E., Berra, E., Gothie, E., Roux, D., Pouyssegur, J., 1999. p42/p44 mitogen-activated protein kinases phosphorylate hypoxia-inducible factor 1alpha (HIF-1alpha) and enhance the transcriptional activity of HIF-1. J. Biol. Chem. 274, 32631–32637.

Robey, P.G., Bianco, P., 2006. The use of adult stem cells in rebuilding the human face. J. Am. Dent. Assoc. 137, 961–972.

Sacchetti, B., Funari, A., Michienzi, S., Di Cesare, S., Piersanti, S., Saggio, I., Tagliafico, E., Ferrari, S., Robey, P.G., Riminucci, M., et al., 2007. Self-renewing osteoprogenitors in bone marrow sinusoids can organize a hematopoietic microenvironment. Cell 131, 324–336.

Sang, N., Stiehl, D.P., Bohensky, J., Leshchinsky, I., Srinivas, V., Caro, J., 2003. MAPK signaling up-regulates the activity of hypoxia-inducible factors by its effects on p300. J. Biol. Chem. 278, 14013–14019.

Semenza, G.L., 2007. Hypoxia-inducible factor 1 (HIF-1) pathway. Sci STKE (2007, cm8).

Sleeman, M., Fraser, J., McDonald, M., Yuan, S., White, D., Grandison, P., Kumble, K., Watson, J.D., Murison, J.G., 2001. Identification of a new fibroblast growth factor receptor, FGFR5. Gene 271, 171–182.

Tondevold, E., Eriksen, J., Jansen, E., 1979. Observations on long bone medullary pressures in relation to arterial PO2, PCO2 and pH in the anaesthetized dog. Acta Orthop. Scand. 50, 645–651.

Tsai, C.C., Chen, Y.J., Yew, T.L., Chen, L.L., Wang, J.Y., Chiu, C.H., Hung, S.C., 2011. Hypoxia inhibits senescence and maintains mesenchymal stem cell properties through down-regulation of E2A-p21 by HIF-TWIST. Blood 117, 459–469.

Volkmer, E., Kallukalam, B.C., Maertz, J., Otto, S., Drosse, I., Polzer, H., Bocker, W., Stengele, M., Docheva, D., Mutschler, W., et al., 2010. Hypoxic preconditioning of human mesenchymal stem cells overcomes hypoxia-induced inhibition of osteogenic differentiation. Tissue Eng. Part A 16, 153–164.

Wang, G.L., Semenza, G.L., 1995. Purification and characterization of hypoxia-inducible factor 1. J. Biol. Chem. 270, 1230–1237.

Wang, G.L., Jiang, B.H., Rue, E.A., Semenza, G.L., 1995. Hypoxia-inducible factor 1 is a basic-helix-loop-helix-PAS heterodimer regulated by cellular O_2 tension. Proc. Natl. Acad. Sci. U. S. A. 92, 5510–5514.

Willam, C., Nicholls, L.G., Ratcliffe, P.J., Pugh, C.W., Maxwell, P.H., 2004. The prolyl hydroxylase enzymes that act as oxygen sensors regulating destruction of hypoxia-inducible factor alpha. Adv. Enzym. Regul. 44, 75–92.

Wotzlaw, C., Otto, T., Berchner-Pfannschmidt, U., Metzen, E., Acker, H., Fandrey, J., 2007. Optical analysis of the HIF-1 complex in living cells by FRET and FRAP. FASEB J. 21, 700–707.

Yoon, J., Deisboeck, T.S., 2009. Investigating differential dynamics of the MAPK signaling cascade using a multi-parametric global sensitivity analysis. PLoS One 4, e4560.

Yu, P.J., Ferrari, G., Galloway, A.C., Mignatti, P., Pintucci, G., 2007. Basic fibroblast growth factor (FGF-2): the high molecular weight forms come of age. J. Cell. Biochem. 100, 1100–1108.

Zhou, M., Sutliff, R.L., Paul, R.J., Lorenz, J.N., Hoying, J.B., Haudenschild, C.C., Yin, M., Coffin, J.D., Kong, L., Kranias, E.G., et al., 1998. Fibroblast growth factor 2 control of vascular tone. Nat. Med. 4, 201–207.